Energy 203 (2020) 117829

Contents lists available at ScienceDirect

Energy

journal homepage: www.elsevier.com/locate/energy

Production of bio-oil with low oxygen and nitrogen contents by combined hydrothermal pretreatment and pyrolysis of sewage sludge

Yali Liu [a, b], Yunbo Zhai [a, b, *], Shanhong Li [a, b], Xiangmin Liu [a, b], Xiaoping Liu [a, b], Bei Wang [a, b], Zhenzi Qiu [a, b], Caiting Li [a, b]

[a] College of Environmental Science and Engineering, Hunan University, Changsha, 410082, PR China
[b] Key Laboratory of Environmental Biology and Pollution Control (Hunan University), Ministry of Education, Changsha, 410082, PR China

ARTICLE INFO

Article history:
Received 4 February 2020
Received in revised form
17 April 2020
Accepted 8 May 2020
Available online 11 May 2020

Keywords:
Hydrothermal pretreatment
Sewage sludge
Temperature
Pyrolysis
Bio-oil

ABSTRACT

In this study, sewage sludge (SS) is first hydrothermally pretreated at 160–250 °C, and subsequently pyrolyzed at 550 °C to produce bio-oil. The effects of the hydrothermal pretreatment (HTP) temperature on the chemical composition, fuel properties, and energy balance of the process are investigated to assess its feasibility. The results show that the characteristics of SS are improved during HTP, including better thermal stability, decreased N content, and enhanced aromaticity, which could influence subsequent pyrolysis. After HTP, the composition of bio-oil shows clear variation. The contents of undesirable O-containing and N-containing compounds, especially acids and amides, are significantly decreased, while the yields of aliphatic hydrocarbons and aromatics increase by 9.53% and 23.18% , respectively. The H/C ratio and higher heating value (HHV) of bio-oil in Sample 190–550 increase to 0.136 and 36.382 MJ/kg, respectively, which are similar to those of biodiesel. The suggested optimal HTP temperature is 190 °C for the HHV and energy recovery rate (44.23%). Meanwhile, the formation pathway of bio-oil with low N and O contents is explored.

1. Introduction

Rapid urbanization and industrial development have caused increasing consumption of fuel and energy. With the increasing depletion of fossil fuels and the environmental problems associated with their use, researching new fuel substitutes and energy sources is increasingly urgent [1]. A variety of biomass resources, including agricultural crops, poultry manure, sewage sludge (SS), and municipal solid waste have been studied for their transformation into biofuel [2–4]. Bora.et al. [5] pointed out that SS, which is enriched in organic materials, is one of the most promising alternative fuel options owing to its low cost, abundant reserves, and readily available sources. With the improvement of sewage treatment capacity and the increasing demand for human activities, the output of SS has surged in the past few decades. It is estimated that by 2020, the output of SS in China will reach approximately 60 million tons per year [6]. Therefore, converting sludge into energy-dense fuels will have great economic and environmental benefits.

Pyrolysis is regarded as an increasingly mature thermochemical process for converting SS into liquid fuels, which is commonly known as bio-oil. In this process, effective volume reduction, pathogen destruction and heavy metal immobilization can also be achieved [7,8]. The study focuses cover the improvement of oil quality [9], reaction mechanism [10] and kinetic analysis [11]. The effects of temperature and gas residence time on the yield and composition of bio-oil from SS pyrolysis have been extensively investigated. Literatures show that prolonging the gas residence time leads to lighter compounds and the highest yield of bio-oil is usually obtained in the range of 450–550 °C [12–14]. However, the resulting bio-oil is difficult to use as transportation fuel owing to its undesirable properties such as high N and O contents, chemical instability and high corrosiveness [15]. Catalytic upgrading of pyrolysis vapors and SS pretreatment for improving feedstock properties prior to pyrolysis are two prevailing approaches to obtain high-quality bio-oil.

Considerable researches have determined that zeolites are one of the most effective catalysts. Wang.et al. [16] reported that HZSM zeolite significantly improves the quality of bio-oil by increasing the yield of aromatic hydrocarbons. The catalytic mechanism of

* Corresponding author. College of Environmental Science and Engineering, Hunan University, Changsha, 410082, PR China.
E-mail address: ybzhai@hnu.edu.cn (Y. Zhai).

https://doi.org/10.1016/j.energy.2020.117829
0360-5442/

different zeolites and the effects of loaded have also been widely studied [17,18]. However, although zeolites show a great effect on the selectively of aromatics, their high price and extreme deactivation limit the development of catalytic pyrolysis.

Most N-containing and O-containing compounds in bio-oil are essentially derived from the decomposition of protein and cellulose in sludge, thus, pretreatment prior to pyrolysis will help to enhance the bio-oil properties, owing to the reduction in O and N in feedstock. Hydrothermal treatment of SS has been demonstrated to convert SS into homogeneous, C-rich solid products (hydrochar) with a lower alkali metal content, lower N and O content [19] and even S element [20].

Recently, many studies have suggested that combining hydrothermal pretreatment (HTP) with pyrolysis of different biomass or low-rank coals has the potential for improving bio-oil quality. For example, Yao.et al. [21] investigated the effect of HTP on fan palm pyrolysis. The authors pointed out that HTP significantly disrupted the chemical structure of fan palms and clearly increased the content of hydrocarbons in bio-oil. Chang.et al. [22] reported that the bio-oil from hydrothermally pretreated eucalyptus wood has lower contents of acids and ketones and an enhanced HHV. Furthermore, Jiang.et al. [23] suggested the oil produced from hydrothermally pretreated oil shale has a higher aliphatic hydrocarbons content. However, the effect of HTP on sludge pyrolysis, and the properties of treated SS-derived bio-oil are rarely mentioned in the literature.

The main purpose of this study is to produce a liquid fuel from SS through combined hydrothermal pretreatment and pyrolysis. The influences of the HTP temperature on the product distribution of bio-oil is investigated. Specifically, comparisons of the composition between water-soluble oil (WSO) and pyrolysis bio-oil are performed to explore the potential routes of N and O reduction and hydrocarbons growth. Finally, the analysis of energy consumption and recovery is conducted to evaluate the feasibility of the process. This work can not only help to understand the effects of HTP on sludge pyrolysis, but also expand the possibilities of preparing bio-oil by sludge.

2. Materials and methods

2.1. Materials preparation

In this study, SS with a moisture content of 88% was obtained from a wastewater treatment plant in Changsha, China. The SS was dried at 80 °C for 48 h and then ground into powder (<80 μm).

2.2. Experimental process

2.2.1. Hydrothermal pretreatment

The HTP process was conducted in a 250 mL autoclave equipped with an automatic temperature controller, pressure gauge and magnetic stirrer. In a typical run, 15.00 ± 0.05 g of SS powder well mixed with 100 mL of deionized water was loaded into the reactor, which was first heated to a preset temperature (160 °C, 190 °C, 220 °C, and 250 °C) and then maintained at this temperature for 30 min. Throughout the hydrothermal process, the magnetic stirrer was rotated at a speed of 200 rpm to ensure that the sludge slurry inside the reactor was homogeneously heated.

Solid and liquid products were separated through negative-pressure filtration. The solid products (hydrochars) were dried until their weight was stable and referred to as HC-temperature, e.g. HC-160 represents hydrochar produced at 160 °C. The filtrate was extracted by CH_2Cl_2 with a volume ratio of 1:5. The oil mixture containing extract was distilled with a rotary evaporator to separate CH_2Cl_2 and WSO, and then the oil sample was marked as WSO-temperature.

2.2.2. Pyrolysis experiments

The pyrolysis experiments were conducted in a tube furnace with a quartz tube of 1200 mm length and 73 mm inner diameter. Approximately 5.000 ± 0.005 g of feedstock loaded into a quartz boat was placed inside the quartz tube. To create an O-free atmosphere before pyrolysis, 0.4 L/min of N_2 was used as the carrier gas and added to the system for 15 min. N_2 was supplied throughout the pyrolysis process to maintain an inert atmosphere. The experiments were performed at 550 °C for 30 min with a heating rate of 10 °C/min. During the reaction, the pyrolysis vapor was condensed with absorption bottles containing acetone in an ice bath. The mixture was then distilled using a rotary evaporator to remove all the acetone and the mass of bio-oil was obtained by calculating the difference of the mass of the distillation flask before and after evaporation. All the bio-oil samples were recorded as X-550, where X indicates the hydrothermal temperature.

2.3. Analytical method

Thermal gravity (TG) and differential thermal gravity (DTG) curves were obtained using a thermogravimetric analyzer (STA 409, NETZSCH, Germany) in an N_2 atmosphere at a heating rate of 10 °C/min. The elemental composition (CHNS) of hydrochars and bio-oil was determined using an elemental analyzer system (Vario MICRO). The O content was then calculated by the difference. Higher heating values (HHVs) were calculated using the elemental composition [24]. The functional groups were analyzed by Fourier transform infrared spectroscopy (FT-IR; Nicolet iN10, Thermo Fisher Scientific). The concentrations of different N-species, including ammonium (NH_4^+-N), nitrate (NO_3^-—N), total nitrogen (TN), and total organic nitrogen (TON) in the liquid phase were measured following previous procedures [25].

The chemical composition of WSO and bio-oil was obtained through an Agilent QP2010 gas chromatograph/mass spectrometer (GC/MS) with an HP-5 MS capillary column. The injection size was 1 μL without splitting. After being maintained at the initial temperature (40 °C) for 2 min, the oven temperature was first raised to 190 °C at a rate of 8 °C/min and then increased to 290 °C at a rate of 6 °C/min, which was held for 8 min. The injector and detector were kept at 280 °C and 230 °C, respectively.

3. Results and discussion

3.1. Effects of hydrothermal pretreatment on sludge characteristics

In this study, hydrochar is an important intermediary linking HTP and subsequent pyrolysis. As the raw material for pyrolysis, the hydrochar characteristics can also influence the bio-oil. Thus, it is necessary to discuss the properties of hydrochars and compare the differences between SS and hydrochars.

3.1.1. Elemental composition of sewage sludge and hydrochars

Table 1 shows the yields of hydrochars under different hydrothermal temperatures and the general properties of SS and hydrochars. The yield of hydrochars decreases to 71.05—79.14% owing to the decomposition of thermally unstable components. The initial O and N contents of SS are 15.05% and 3.00%, respectively. With elevated HTP temperature, the percentages of O and N in the hydrochars gradually decrease to 3.10% and 0.96%, respectively, at 250 °C. The reasonable explanation for this is that O-containing and N-containing functional groups are transferred into

Table 1
Contents of the main elements and properties of the sewage sludge (SS) and hydrochars.

Samples	Yield (%)	Proximate Analysis (%)			Ultimate Analysis (%)					Atomic Ratio	
		A	VM	FC	C	H	N	S	O[a]	H/C	O/C
SS	/	57.78	41.14	1.08	20.34	3.39	3.00	0.44	15.05	1.99	0.56
HC-160	79.14	62.33	36.39	1.28	18.81	2.65	1.68	0.59	9.24	1.69	0.37
HC-190	75.24	73.33	24.84	1.83	15.91	2.21	1.42	0.56	6.57	1.67	0.31
HC-220	71.24	74.29	22.60	3.11	16.11	2.17	1.11	0.53	5.80	1.62	0.27
HC-250	71.05	76.12	19.50	4.38	17.50	2.04	0.96	0.38	3.10	1.40	0.13

A, ash.
VM, volatile matter.
FC, fixed carbon.
[a], calculated by difference: O% = 100-C%-H%-N%-S%-Ash%.

air or liquid in the form of CO_2, H_2O, and NH_4^+ during hydrothermal process [26,27], which can help to reduce the formation of O-containing and N-containing compounds during subsequent pyrolysis. The decreased H/C and O/C ratios demonstrate the enhancement of the decarboxylation and dehydration reactions [28]. The ash content of the hydrochars clearly increased, but the reduction of elemental C is weakened with increasing temperature, indicating that the carbonization reaction occurs at a relatively higher temperature, and thus some carbons are converted into the form of fixed carbon.

3.1.2. Functional group characteristics of SS and hydrochars

The FT-IR spectra of the raw SS and hydrochars are shown in Fig. 1. It is clear that the main functional groups in the SS and hydrochars remain the same, but their intensity has changed. The broad bands in the range of 3600 cm^{-1} and 3200 cm^{-1} are ascribed to stretching of the −OH bond in carboxyl and hydroxyl groups [29]. The intensity of −OH decreases after the HTP process, indicating the dehydration reaction was probably facilitated. Compared with that of the unpretreated SS, a clear reduction in the peaks at 1640 cm^{-1}, namely the amide I band [30] (C═O absorption vibration), and at 1540 cm^{-1}, namely the amide II band [28] (N−H bending vibration) could be observed for hydrochars, revealing the degradation of protein, and the result is in line with that of elemental analysis. The reduced organic-N is transformed into the liquid phase in the form of NO_3^- and NH_4^+ (Fig. S1). Moreover, the

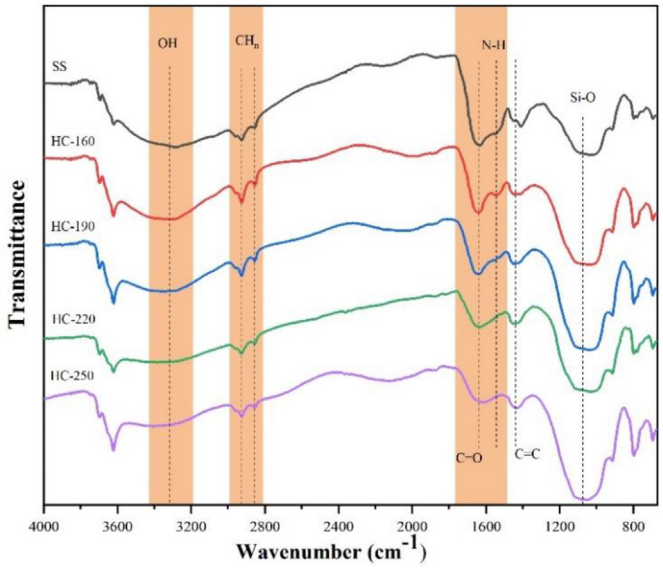

Fig. 1. Fourier transform infrared spectroscopy of SS and hydrochars.

intensity of the peaks at 2925 cm^{-1} and 2855 cm^{-1}, which correspond to the aliphatic carbon $-CH_2-$ stretching vibration, show a slight increase. This is attributed to the exchange between hydrogen and O-containing functional groups [31]. The band near 1440 cm^{-1} related to the aromatic C═C vibration exhibits increased intensity with increasing temperature, indicating that the aromaticity of hydrochars is enhanced compared with that of SS [24]. Thus, HTP helps to promote the removal of N and O contents and enhance the degree of aromaticity of SS.

3.1.3. Thermal characteristics analysis of SS and hydrochars

Fig. 2 shows the TG and DTG curves of SS and hydrochars at different HTP temperatures. Three clear temperature stages could be found. Stages a, b, and c are the dehydration, devolatilization and carbonization stages, respectively. In this study, the decomposition of volatiles mainly occurs in the temperature range of 150−550 °C, where 12.87%−32.55% weight loss occurred, and two clear peaks in the DTG curve in this temperature range are observed. With the increase in the HTP temperature, the first peak of the DTG curve is gradually weakened, while the second peak becomes clearer. Moreover, unlike the two DTG peaks between 150 and 550 °C of the other three samples, only a single peak can be observed in the HC-250 sample. This could be ascribed to the reduction in light volatile matter and the increment in fixed carbon. When the temperature exceeds 550 °C, continued increase in temperature has little effect on mass loss, indicating the volatiles have almost completely evaporated. Thus, 550 °C was chosen as the pyrolysis temperature.

3.1.4. Pyrolysis kinetics analysis

In order to determine the effects of HTP on the pyrolysis characteristics, the Coast-Redfern model is used to determine the activation energy (E) of the thermal decomposition process. The reaction kinetics of pyrolysis can be described by Eqs. (1) and (2), where β is the heating rate, W_0, W_t, W_∞ indicate initial, instantaneous, and residue mass respectively.

$$\frac{d\alpha}{dT} = \frac{1}{\beta} K(T) f(\alpha) \tag{1}$$

$$\alpha = \frac{W_0 - W_t}{W_0 - W_\infty} \tag{2}$$

Following the Arrhenius formula ($K = A \cdot exp\left(\frac{-E}{RT}\right)$), where R is a gas constant (R = 8.314 $J \cdot mol^{-1} \cdot K^{-1}$), T is the absolute temperature (K), and A is a pre-exponential factor (min^{-1}), Eq. (1) can be expressed as Eq. (3).

$$\frac{d\alpha}{dT} = \frac{A}{\beta} exp\left(\frac{-E}{RT}\right) f(\alpha) \tag{3}$$

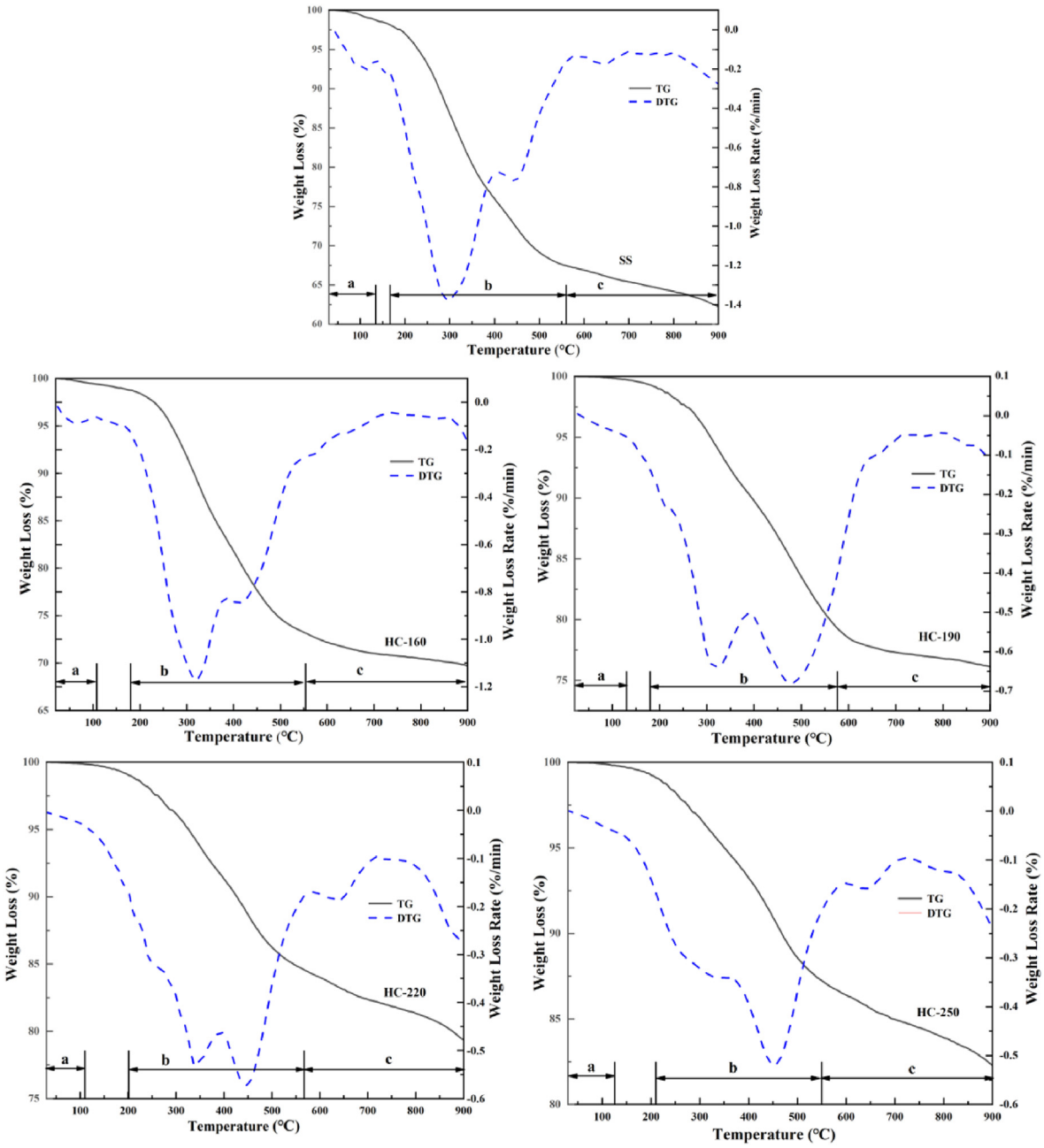

Fig. 2. TG-DTG pyrolysis curves of hydrochars at different temperature.

Using the integral equation method, Eq. (3) can be transformed into Eq. (4).

$$\int_0^{\alpha} \frac{1}{f(\alpha)} d\alpha = g(\alpha) = \frac{A}{\beta} \int_0^{T} exp\left(\frac{-E}{RT}\right) dT \tag{4}$$

Assuming that the pyrolysis process is a simple reaction with a reaction order of 1, the conversion function can be described as follows: $f(\alpha) = (1-\alpha)^n$, where n = 1.

Integration of Eq. (5) gives the following:

$$\ln\left[-\frac{\ln(1-\alpha)}{T^2}\right] = \ln\left[\frac{AR}{\beta E}\left(1-\frac{2RT}{E}\right)\right] - \frac{E}{RT} \tag{5}$$

Generally, $\frac{RT}{E} \ll 1$, so Eq. (5) can be simplified as follows:

$$\ln\left[-\frac{\ln(1-\alpha)}{T^2}\right] = \ln\left(\frac{AR}{\beta E}\right) - \frac{E}{RT} \tag{6}$$

Therefore, the plot between $^1/_T$ and $\ln[-\ln(1-\alpha)/T^2]$ is a straight line, and the E and A can be calculated from the slope and intercept.

Table 2
Pyrolysis kinetic parameters of SS and hydrochars.

Samples	Temperature (°C)	E (kJ/mol)	A (min^{-1})	R^2
SS	154–409	33.19	7.22	0.9626
	409–559	16.04	2.02	0.9669
HC-160	180–390	49.65	15.79	0.9573
	370–530	35.95	7.63	0.9788
HC-190	226–397	44.34	7.64	0.9818
	397–577	61.51	16.00	0.9755
HC-220	201–401	36.69	4.68	0.9951
	401–567	40.92	6.20	0.9664
HC-250	210–355	37.23	4.64	0.9893
	355–547	15.01	1.84	0.9749

In this study, kinetics analysis only focuses on the two pyrolysis zones of the devolatilization stage, i.e., the temperature ranges of approximately 150–400 °C and 400–550 °C. The E and A are calculated by Eq. (6), as shown in Table 2. The correlation coefficient (R^2) ranging from 0.9626 to 0.9951 indicates that the pyrolysis process can be successfully fitted by the reaction model. The E values of the first zone are higher than those of the second zone in the HC-160 and HC-190 samples, while they are lower in the HC-220 and HC-250 samples, indicating the substrates become increasingly reactive in the first zone with the rising HTP temperature. As for the hydrochars, E and A of the first zone in the HC-160 sample are the highest with values of 49.65 kJ/mol and 15.79 min^{-1}, respectively. This might have been due to the continuous decrease in light volatile matter. A similar result is found in the research of Zhou et al. [32]. When the HTP temperature reaches 190 °C, the E value of the second pyrolysis zone increases to 45.47 kJ/mol and then decreases slightly with the continuous increase in temperature. Overall, compared with that of SS, the E values for the pyrolysis zone in hydrochars are relatively higher, indicating that HTP improves the stability of SS, which will have better performance for storage and transportation.

3.2. Effects of hydrothermal pretreatment on the quality of bio-oil

Bio-oil samples derived from SS and hydrochar pyrolysis are mixtures of complex compounds, the compositions of which can vary. In order to clarify their differences, detailed characterization of bio-oil and a comparison between WSO and bio-oil are performed to reveal the effect of HTP on SS.

3.2.1. Functional group characteristics of bio-oil and water-soluble oil

The FTIR spectra of WSO and bio-oil are shown in Fig. 3 (a) and (b). The similar absorption peaks confirmed that they contained similar functional groups, however, conspicuous differences in intensities could be observed. In the WSO, the stretching vibration of C═O groups is the most pronounced, suggesting that the amide and ketone groups account for a large proportion of the components [33]. Moreover, the intensity of $-CH_2-$ in WSO is weak, while it is much clearer in bio-oil. This difference is further widened with increasing temperature. Compared with bio-oil produced by SS, the stretching vibration of −OH at 3400 cm^{-1} in other four samples are weakened. The FTIR results of bio-oil are in accordance with those of hydrochars, demonstrating that improved feedstock properties can cause changes in the properties of derived bio-oil. It is worth noting that the vibration of C≡N appearing at approximately 2200 cm^{-1} could only be found in the bio-oil sample from SS pyrolysis. In general, the FTIR results showed that the quality of the bio-oil could be improved by HTP, but the specific impacts of different HTP temperatures need to be discussed further.

3.2.2. Composition characteristics of bio-oil and water-soluble oil

The chemical compositions of WSO and bio-oil are determined by GC/MS. These two types of oil are complex mixtures of different chemical compounds, mainly including aliphatic hydrocarbons, aromatics, O-containing compounds, and N-containing compounds, as shown in Fig. 4. It is clear that HTP has a significant effect on the bio-oil composition. When SS is pyrolyzed, high percentages of O-containing compounds (43.39%) and N-containing compounds (39.80%) are found in the bio-oil. With the increase in the HTP temperature, the content of O-containing compounds in both WSO and bio-oil gradually decreases, which is mainly ascribed to the intensified degree of dehydration and decarboxylation reactions. In addition, the reduction in N-containing compounds in bio-oil is in accordance with the steadily increasing trend in WSO. This evolution indicates that some N-containing components are converted into other N-species, which are then easily enriched in the WSO. Furthermore, the increasing trend of O-containing and N-containing compounds in WSO starts to be gentle when temperature reaches 220 °C.

It can be speculated that the HTP process is conducive to the

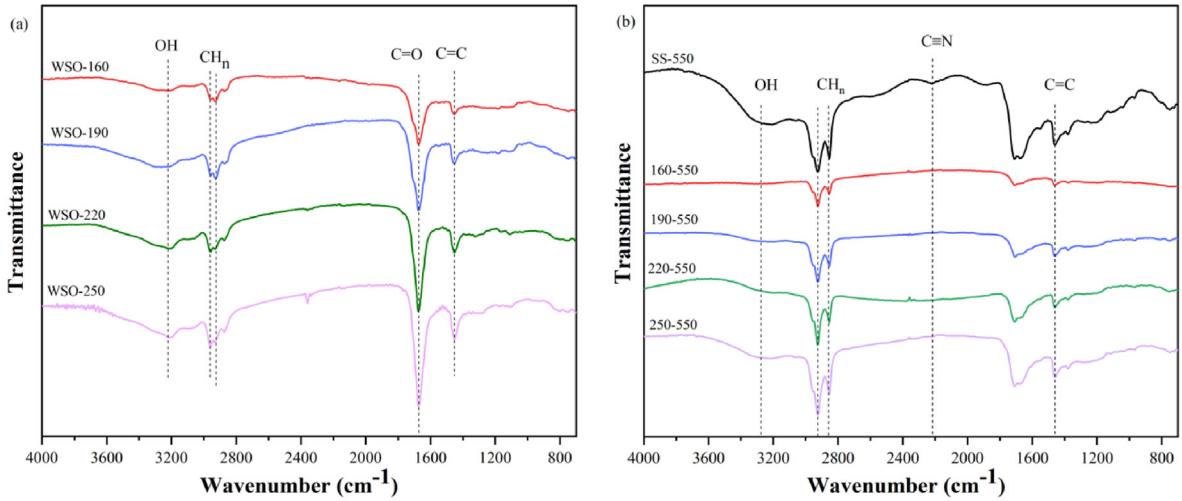

Fig. 3. Fourier transform infrared spectroscopy of (a) water-soluble oil (WSO) and (b) bio-oil from SS and hydrochars.

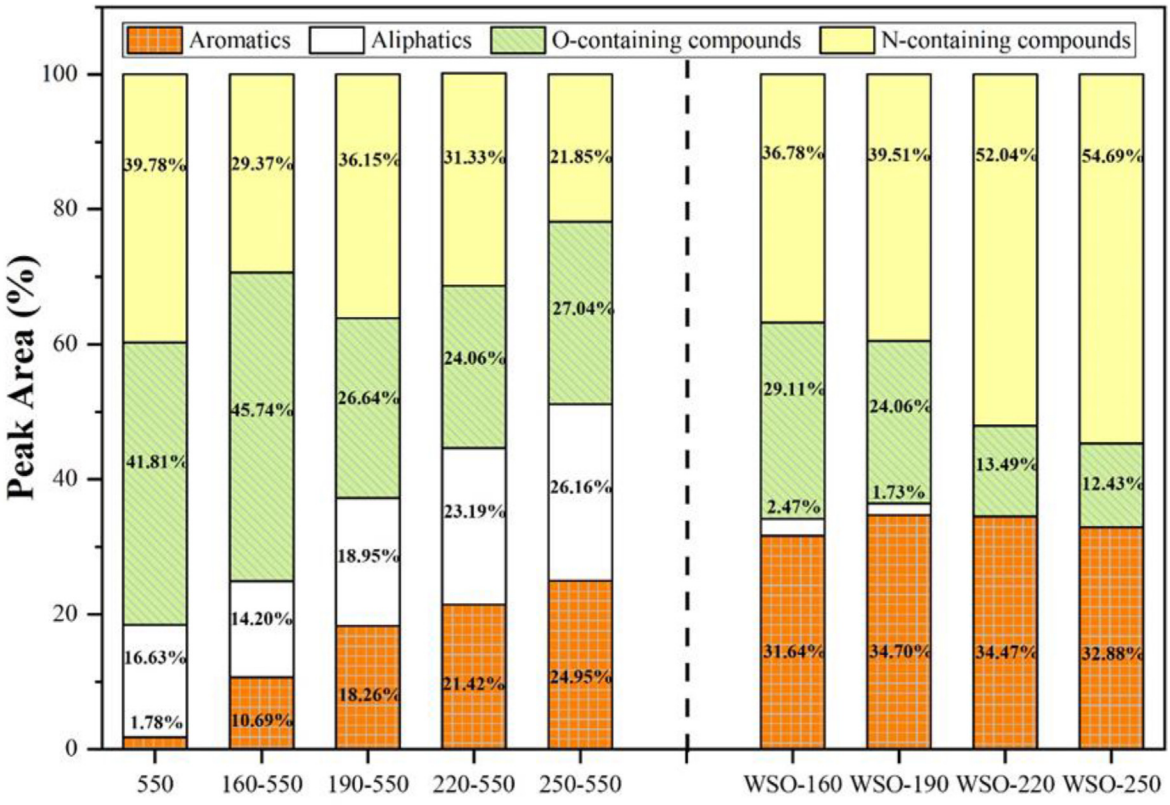

Fig. 4. Component distribution of water-soluble oil (WSO) and bio-oil from SS and hydrochars.

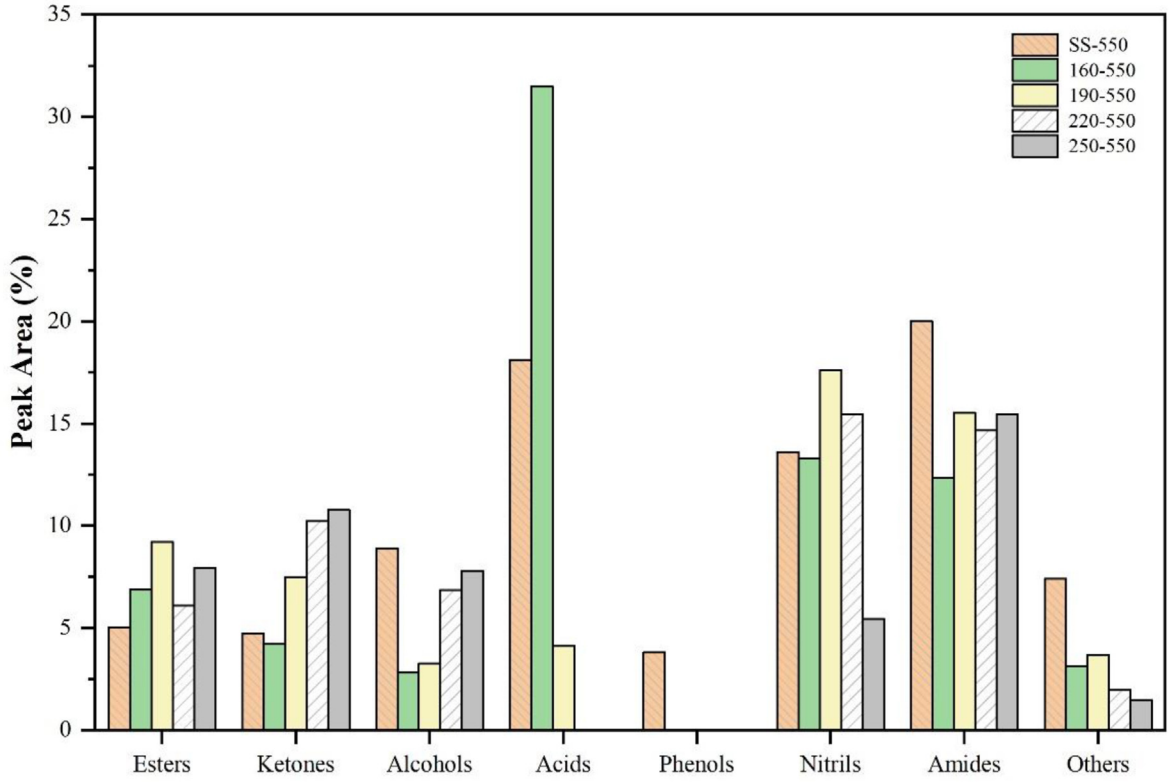

Fig. 5. O-containing and N-containing compound distribution on bio-oil from pyrolysis of SS and hydrochars.

generation of hydrocarbons in the pyrolysis stage, as the content of hydrocarbons in bio-oil increases steadily from 16.81% to 51.11% with elevated HTP temperatures, in which aliphatic hydrocarbons and aromatics increased by 9.53% and 23.18% respectively. However, the hydrocarbons content in WSO is barely affected. On one hand, the aliphatic carbon of side chains is more easily broken during pyrolysis after HTP [31], thereby resulting in the generation of aliphatic hydrocarbons. On the other hand, the decomposition of some complex macromolecular compounds, such as fatty acids, also generates hydrocarbons [19].

Aromatic hydrocarbons are desirable components of liquid products owing to their high energy density and stability. A negligible amount of aromatics exists in the bio-oil from SS pyrolysis, however, a clear increase in aromatics is found in the hydrochar-derived bio-oil, and similar finding is reported in the pyrolysis of hydrothermal treated digested sludge [34]. The results demonstrated that the quality of bio-oil as a liquid fuel is improved by HTP. Researches have shown that HTP can promote chain breaking and cracking reactions of carbohydrates to form some oxygenates and olefins, which are easily cyclized with SS-derived olefins to form benzene aromatics by the Diels-Alder and dehydration reactions [35,36]. Detailed compound distribution of hydrocarbons in bio-oil is given in Table S1. The types of aliphatic hydrocarbons are clearly reduced, indicating the composition of bio-oil from hydrochars is simplified and is purer. For example, in the hydrochar-derived bio-oil, heneicosane ($C_{21}H_{44}$), 1-nonadecene ($C_{19}H_{38}$) and 9-tricosene, (E)- ($C_{23}H_{46}$), which are diesel-type distillates in the range of C_{13}–C_{25} [37], increase significantly and become the predominant components, while more types of hydrocarbons with a low content in SS-derived bio-oil are observed. The alkane content slightly fluctuates, while the proportion of alkenes and aromatics in bio-oil from hydrochar increases. It is inferred that alkenes can be produced from direct cracking of aliphatic side chain. These alkenes may subsequently be converted into to aromatics through cyclization [38].

To further determine the distribution of O-containing and N-containing compounds in bio-oil, we classified them into eight groups based on functional groups (fatty acids, alcohols, esters, phenols, nitriles, amides and others including amines, furans, and N-containing heterocycles). The sums of each group are presented in Fig. 5 as a percentage of peak area.

A high proportion of nitrogenous compounds (14.61% of nitriles and 21.00% of amides) is detected in the SS-550 sample. The nitriles content slightly fluctuates in the first four samples but suddenly decreases to 5.45% in the 250–550 sample. It is speculated that the HTP process at 250 °C promotes the hydrolysis of nitriles to acids and ammonia (NH_3) [39]. N in the WSO exists in the form of cyclic compounds which are basically absent or negligible in the bio-oil. However, long-chain amides still remain in the bio-oil. As shown in Table S2, cyclic lactams account for a large portion of 39.23–45.23% and are the predominant nitrogenous compounds in the WSO, the rest are compounds such as pyrrole, pyrazine and pyridin. The Maillard reaction should be responsible for generating N-containing heterocycles from amino-N [33].

Table 3
Characteristics of bio-oil from SS and hydrochars.

Samples	Elemental Analysis (%)					HHV (*MJ/kg*)
	C	H	N	S	O[a]	
SS-550	68.23	8.722	7.89	0.723	14.435	32.972
160–550	72.31	10.838	6.01	0.112	10.730	36.899
190–550	73.60	10.011	5.22	0.308	10.861	36.382
220–550	74.20	9.802	4.68	0.415	10.903	36.353
250–550	75.12	9.968	3.62	0.568	10.724	37.007

[a] , calculated by difference: O% = 100-C%-H%-N%-S%.

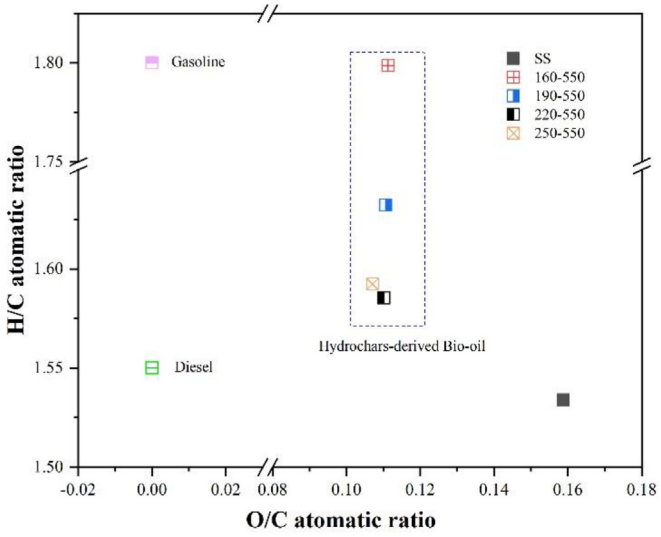

Fig. 6. Van Krevelen diagram of bio-oil obtained from SS and hydrochars.

As for the oxygenates, the content of acids increases from 19.92% to 31.49% after HTP under 160 °C, which is followed by a sharp decrease until disappearing with further temperature elevation. As discussed in previous literature, most liable proteins and lipids are prone to hydrolysis at 150 °C, leading to the release of organic acids [27]. These fatty acids can generate a large number of long-chain hydrocarbons through decarboxylation in a hydrothermal environment [40]. The results are consistent with the high aliphatic hydrocarbon content in Samples 220–550 and 250–550. Increased ketones may also be related to the decrease in acid yield, as the ketonization reaction can remove carboxyl groups and convert acids into ketones. The sharp reduction in the acids content indicated that the bio-oil is less corrosive and more stable. In general, the bio-oil obtained from hydrochars has better quality with reduced N-heterocycles contents and increased hydrocarbon contents, and the hydrothermal temperature of 250 °C exerts the greatest effects.

3.2.3. Elemental composition of bio-oil

Elemental analysis is performed to measure the energy density and combustion performance of bio-oil. Because our target product is pyrolysis bio-oil instead of WSO, only bio-oil results are discussed in this section. Table 3 shows the elemental analysis results of the bio-oil from SS and hydrochars.

After HTP, the obtained bio-oil has higher contents of C and H, while the O and N contents are lower compared with those of the bio-oil from SS, especially N. The N content in the bio-oil is gradually reduced with elevated HTP temperature, and the maximum removal efficiency of N reaches 54.12% at 250 °C. This could be attributed to the improvement of raw material performance through the HTP process.

In addition, the H/C and O/C atomic ratios are important indicators to evaluate bio-oil performance. Fig. 6 shows the atomic ratios for the bio-oil samples obtained under different pretreatment temperatures. As shown in Fig. 6, the O/C ratio in the bio-oil from hydrochars is clearly lower than that from SS. The H/C ratio increases from 1.534 to 1.585–1.799, suggesting the obtained bio-oil possesses higher energy content [41]. The H/C ratios of 190–550, 220–550, and 250–550 exceed that of biodiesel (1.55), and the ratio of 160–550 is even closed to that of gasoline (1.80) [42]. From this perspective, we believe that the bio-oil produced by SS has great potential for application. As the hydrothermal

Table 4
Energy balance during bio-oil production.

Sample	Input in HTP (MJ)	Input in Pyrolysis (MJ)	Total Input (MJ)	Total Output (KJ)	Energy Recovery Rate (%)
SS-550	/	844	844.00	62.70	43.66
160–550	98.06	844	942.06	56.38	39.26
190–550	113.97	844	957.97	63.52	44.23
220–550	128.91	844	972.91	35.86	24.97
250–550	142.47	844	986.47	29.58	20.61

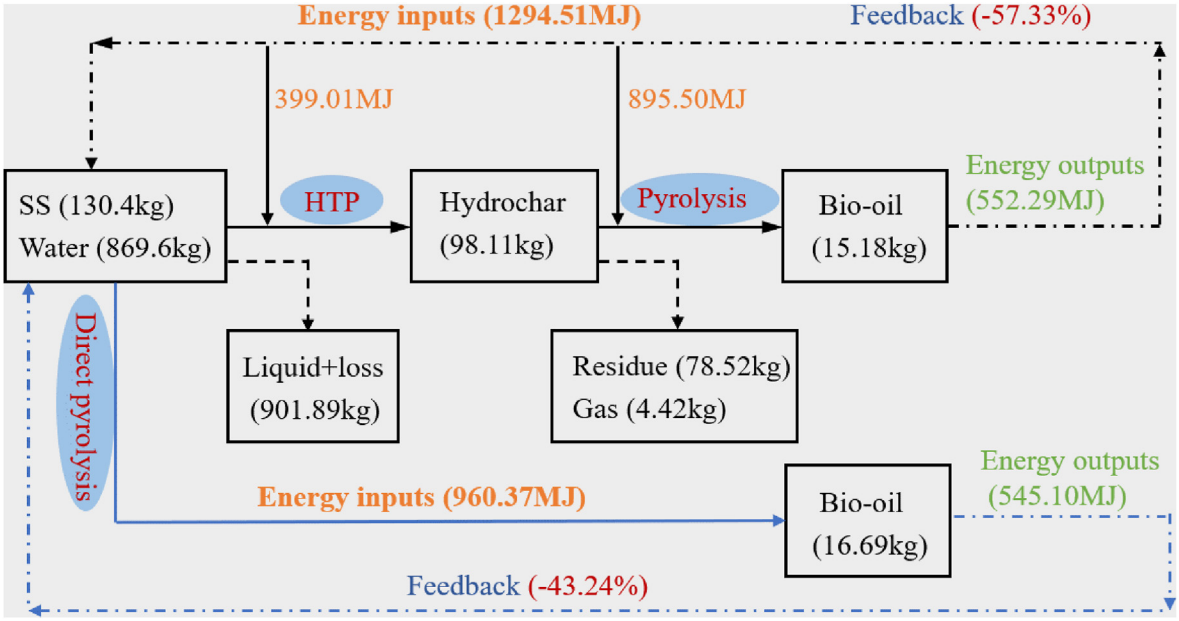

Fig. 7. Mass and energy balance of bio-oil production.

temperature increased, the proportion of C atoms increases gradually, but the H/C value decreases significantly, which might have been caused by cyclization or secondary cleavage of aliphatic compounds at higher temperatures. The HHV of bio-oil from hydrochars is barely affected by the variation in HTP temperature, and remains stable at 36.353–37.007 MJ/kg, however, it is generally higher than that of bio-oil from SS. Also, compared with the oil products obtained through other methods, the bio-oil still has better fuel performance. For example, Huang et al. [43] obtained the bio-oil through co-liquefaction of SS and rice straw at 350 °C, which has obviously higher O contents (65.7% C, 8.3% H, 4.5% N, 21.2% O and 0.3% S). Zhou et al. [44] also obtained a liquid fuel (47.61% C, 10.62% H, 6.16% N and 35.61% O) through a microwave pyrolysis system at 500 °C with a lower HHV (20.61 MJ/kg). Overall, HTP can help to remove heteroatoms of bio-oil and improve its fuel performance.

3.2.4. Mass and energy balance

In order to intuitively compare the yield of the product with or without HTP, we considered the total mass of all samples to be 115 g (15 g of SS and 100 g of water). The mass balance analysis for the whole process is given in Table S3. The yield of bio-oil is reduced by varying degrees after HTP, and the minimum loss occurs at 190 °C. Based on the mass balance and the heating values of the solid and liquid products, the energy balance is performed with reference to the research conducted by Peng et al. [45]. More details are provided in Text S1. As presented in Table 4, the highest energy recovery rate of 44.23% is obtained after HTP at 190 °C. However, the total energy input is far greater than the energy output, as the energy consumption of the machine will be relatively higher at the laboratory scale. Fig. 7 illustrates the energy flow through the process (capacity of 1 t/batch) with HTP at 190 °C. The energy utilization efficiency is significantly improved with increasing scale. In the current condition, the energy from the bio-oil combustion reaches 42.67% of the total input energy, which could be recycled to supplying heat for the process. Therefore, the energy consumption could be lower in practical application with increasing reactor scale, thereby resulting in recycling of more energy output.

3.3. Formation pathway of bio-oil with low nitrogen and oxygen

Based on the aforementioned analysis with relevant references, the potential removal routes of N and O through HTP are presented in Fig. 8. During the HTP process, the majority of organic N is transformed into the liquid phase in the form of NH_4^+ and NO_3^-. On the other hand, ring condensation of amino-N leads to increased N-heterocycles, which are easily transferred into the WSO [33]. These are the two main pathways for reducing the N content in bio-oil. In addition, partial hydrolysis of nitriles which occurs at 250 °C with the formation of acids and ammonia also helps to reduce the N content [39]. HTP facilitates the chain breaking of carbohydrates in SS and then different types of oxygenates are released. These oxygenates, particularly alcohols and acids, can generate long-chain aliphatic hydrocarbons by dehydration and decarboxylation, which is the main source of increased aliphatic hydrocarbons in the bio-oil [40]. In addition, the aliphatic C of side chains is more easily broken during pyrolysis after HTP [31], which is also responsible for the increase in alkenes. Furans derived from SS can react with

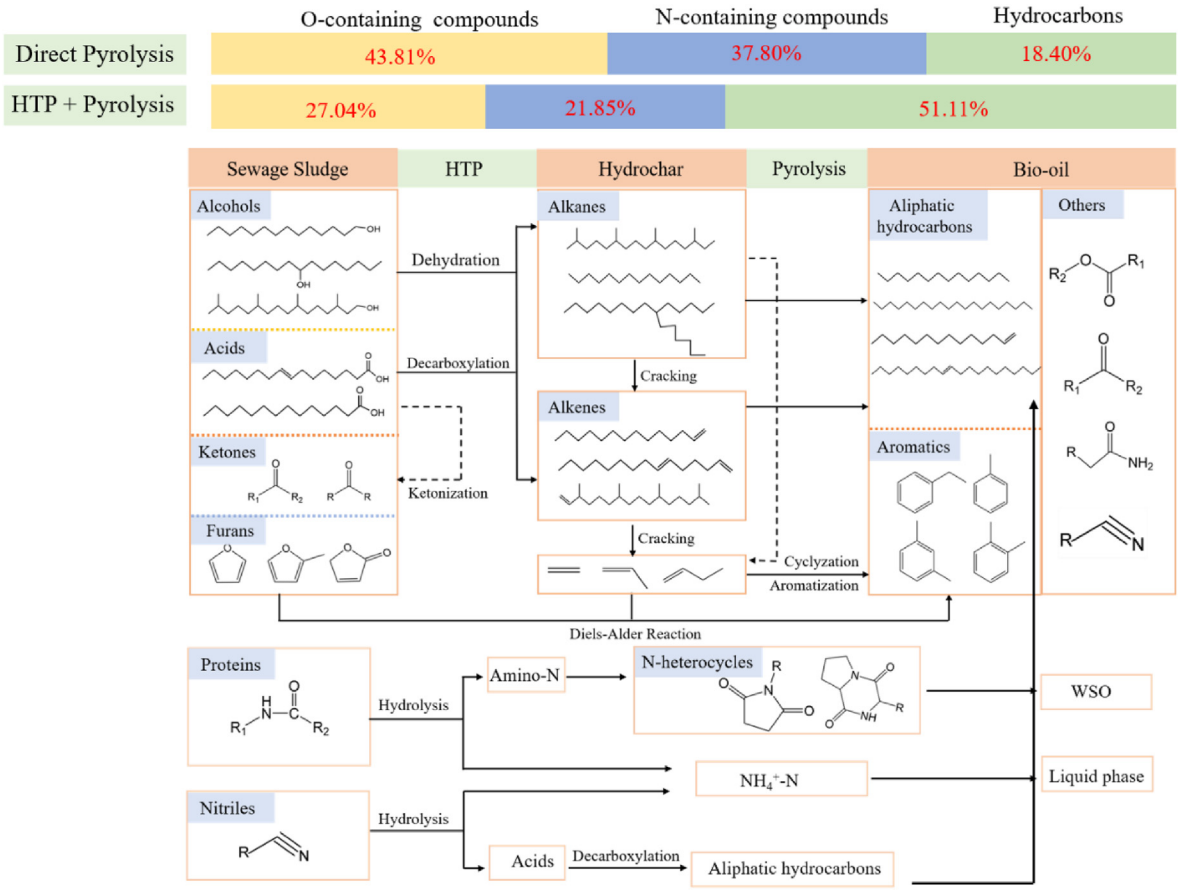

Fig. 8. Formation pathway of bio-oil with low N and O contents.

alkenes through the Diels-Alder reaction to form monocyclic aromatics [36]. The cyclization and aromatization of alkenes is another important pathway for the formation of monocyclic aromatics. Finally, clearly improved bio-oil with less O-containing and N-containing compounds and more hydrocarbons is obtained.

4. Conclusions

Liquid fuel is expected to be produced from SS through a combined HTP and pyrolysis process. This study preliminarily investigates the effects of the HTP temperature on the chemical properties of bio-oil. The comprehensive characteristics of the hydrochars and bio-oil are determined. Furthermore, energy consumption and recovery of the whole process are calculated to estimate the feasibility of bio-oil production. The main conclusions are as follows:

(1) HTP significantly influences the chemical composition of bio-oil. The HTP process promotes deoxygenation and denitrification. The contents of O-containing and N-containing compounds in bio-oil produced from hydrochars are reduced, while the contents of aliphatic hydrocarbons and aromatics are significantly enhanced. The highest removal efficiency (17.93%) of total N-containing compounds in bio-oil is observed in Sample 250–550.
(2) The pathway of organic conversion is influenced by HTP. Lactams-N and heterocyclic-N compounds from the cracking of protein are transferred into WSO during HTP. HTP enhances the decarboxylation reaction of fatty acids, thereby leading to an increase in aliphatic hydrocarbons.
(3) The HHV of hydrochar-derived bio-oil is higher than that of SS, however, it is barely affected by the variation in HTP temperature, and remains stable at 36.353–37.007 MJ/kg. The H/C and O/C ratios show that the characteristics of bio-oil from SS are similar to those of biodiesel. According to the energy balance, the highest energy recovery rate of 44.23% is obtained after HTP at 190 °C. Taking into account the bio-oil quality and energy saving, the optimal HTP temperature for bio-oil production is 190 °C.

Declaration of competing interest

The authors declare that they have no known competing financial interests or personal relationships that could have appeared to influence the work reported in this paper.

CRediT authorship contribution statement

Yali Liu: Conceptualization, Investigation, Formal analysis, Methodology, Validation, Writing - original draft, Writing - review & editing. **Yunbo Zhai:** Supervision, Funding acquisition. **Shanhong Li:** Resources, Project administration. **Xiangmin Liu:** Writing - review & editing, Data curation. **Xiaoping Liu:** Formal analysis. **Bei Wang:** Writing - review & editing. **Zhenzi Qiu:** Investigation, Formal analysis. **Caiting Li:** Project administration, Resources.

Acknowledgement

This research was financially supported by a key research and development project of Hunan Province (2018WK2010,2018WK2011) and a project of the National Natural Science Foundation of China (No. 51679083).

Appendix A. Supplementary data

Supplementary data to this article can be found online at https://doi.org/10.1016/j.energy.2020.117829.

References

[1] Raheem A, Sikarwar VS, He J, Dastyar W, Dionysiou DD, Wang W, Zhao M. Opportunities and challenges in sustainable treatment and resource reuse of sewage sludge: a review. Chem Eng J 2018;337:616–41. https://doi.org/10.1016/j.cej.2017.12.149.
[2] Wang T, Zhai Y, Zhu Y, Li C, Zeng G. A review of the hydrothermal carbonization of biomass waste for hydrochar formation: process conditions, fundamentals, and physicochemical properties. Renew Sustain Energy Rev 2018;90:223–47. https://doi.org/10.1016/j.rser.2018.03.071.
[3] Çolak U, Durak H, Genel S. Hydrothermal liquefaction of Syrian mesquite (Prosopis farcta): effects of operating parameters on product yields and characterization by different analysis methods. J Supercrit Fluids 2018;140:53–61. https://doi.org/10.1016/j.supflu.2018.05.027.
[4] Durak H. Hydrothermal liquefaction of Glycyrrhiza glabra L. (Liquorice): effects of catalyst on variety compounds and chromatographic characterization, energy sources, Part A: recovery, utilization, and environmental effects. 2019. p. 1–14. https://doi.org/10.1080/15567036.2019.1607947.
[5] Bora AP, Gupta DP, Durbha KS. Sewage sludge to bio-fuel: a review on the sustainable approach of transforming sewage waste to alternative fuel. Fuel 2020;259. https://doi.org/10.1016/j.fuel.2019.116262.
[6] Lishan X, Tao L, Yin W, Zhilong Y, Jiangfu L. Comparative life cycle assessment of sludge management: a case study of Xiamen, China. J Clean Prod 2018;192:354–63. https://doi.org/10.1016/j.jclepro.2018.04.171.
[7] Syed-Hassan SSA, Wang Y, Hu S, Su S, Xiang J. Thermochemical processing of sewage sludge to energy and fuel: fundamentals, challenges and considerations. Renew Sustain Energy Rev 2017;80:888–913. https://doi.org/10.1016/j.rser.2017.05.262.
[8] Chen G, Tian S, Liu B, Hu M, Ma W, Li X. Stabilization of heavy metals during co-pyrolysis of sewage sludge and excavated waste. Waste Manag 2020;103:268–75. https://doi.org/10.1016/j.wasman.2019.12.031.
[9] Sharifzadeh M, Sadeqzadeh M, Guo M, Borhani TN, Murthy Konda NVSN, Garcia MC, Wang L, Hallett J, Shah N. The multi-scale challenges of biomass fast pyrolysis and bio-oil upgrading: review of the state of art and future research directions. Prog Energy Combust Sci 2019;71:1–80. https://doi.org/10.1016/j.pecs.2018.10.006.
[10] Luo J, Ma R, Huang X, Sun S, Wang H. Bio-fuels generation and the heat conversion mechanisms in different microwave pyrolysis modes of sludge. Appl Energy 2020;266. https://doi.org/10.1016/j.apenergy.2020.114855.
[11] Tang S, Zheng C, Zhang Z. Effect of inherent minerals on sewage sludge pyrolysis: product characteristics, kinetics and thermodynamics. Waste Manag 2018;80:175–85. https://doi.org/10.1016/j.wasman.2018.09.012.
[12] Shen L, Zhang D-K. An experimental study of oil recovery from sewage sludge by low-temperature pyrolysis in a fluidised-bed☆. Fuel 2003;82(4):465–72.
[13] Alvarez J, Lopez G, Amutio M, Artetxe M, Barbarias I, Arregi A, Bilbao J, Olazar M. Characterization of the bio-oil obtained by fast pyrolysis of sewage sludge in a conical spouted bed reactor. Fuel Process Technol 2016;149:169–75. https://doi.org/10.1016/j.fuproc.2016.04.015.
[14] Gerasimov G, Khaskhachikh V, Potapov O, Dvoskin G, Kornileva V, Dudkina L. Pyrolysis of sewage sludge by solid heat carrier. Waste Manag 2019;87:218–27. https://doi.org/10.1016/j.wasman.2019.02.016.
[15] Chen Y, Zhang L, Zhang Y, Li A. Pressurized pyrolysis of sewage sludge: process performance and products characterization. J Anal Appl Pyrol 2019;139:205–12. https://doi.org/10.1016/j.jaap.2019.02.007.
[16] Wang K, Zheng Y, Zhu X, Brewer CE, Brown RC. Ex-situ catalytic pyrolysis of wastewater sewage sludge - a micro-pyrolysis study. Bioresour Technol 2017;232:229–34. https://doi.org/10.1016/j.biortech.2017.02.015.
[17] Wei F, Cao J-P, Zhao X-Y, Ren J, Gu B, Wei X-Y. Formation of aromatics and removal of nitrogen in catalytic fast pyrolysis of sewage sludge: a study of sewage sludge and model amino acids. Fuel 2018;218:148–54. https://doi.org/10.1016/j.fuel.2018.01.025.
[18] Gu B, Cao J-P, Wei F, Zhao X-Y, Ren X-Y, Zhu C, Guo Z-X, Bai J, Shen W-Z, Wei X-Y. Nitrogen migration mechanism and formation of aromatics during catalytic fast pyrolysis of sewage sludge over metal-loaded HZSM-5. Fuel 2019;244:151–8. https://doi.org/10.1016/j.fuel.2019.02.005.
[19] Zhao P, Shen Y, Ge S, Chen Z, Yoshikawa K. Clean solid biofuel production from high moisture content waste biomass employing hydrothermal treatment. Appl Energy 2014;131:345–67. https://doi.org/10.1016/j.apenergy.2014.06.038.
[20] Wang Z, Zhai Y, Wang T, Peng C, Li S, Wang B, Liu X, Li C. Effect of temperature on the sulfur fate during hydrothermal carbonization of sewage sludge. Environ Pollut 2020;260:114067. https://doi.org/10.1016/j.envpol.2020.114067.
[21] Yao Z, Ma X. Effects of hydrothermal treatment on the pyrolysis behavior of Chinese fan palm. Bioresour Technol 2018;247:504–12. https://doi.org/10.1016/j.biortech.2017.09.142.
[22] Chang S, Zhao Z, Zheng A, Li X, Wang X, Huang Z, He F, Li H. Effect of hydrothermal pretreatment on properties of bio-oil produced from fast pyrolysis of eucalyptus wood in a fluidized bed reactor. Bioresour Technol 2013;138:321–8. https://doi.org/10.1016/j.biortech.2013.03.170.
[23] Jiang H, Deng S, Chen J, Zhang M, Li S, Shao Y, Yang J, Li J. Effect of hydrothermal pretreatment on product distribution and characteristics of oil produced by the pyrolysis of Huadian oil shale. Energy Convers Manag 2017;143:505–12. https://doi.org/10.1016/j.enconman.2017.04.037.
[24] Peng C, Zhai Y, Zhu Y, Xu B, Wang T, Li C, Zeng G. Production of char from sewage sludge employing hydrothermal carbonization: char properties, combustion behavior and thermal characteristics. Fuel 2016;176:110–8. https://doi.org/10.1016/j.fuel.2016.02.068.
[25] Xiao H, Zhai Y, Xie J, Wang T, Wang B, Li S, Li C. Speciation and transformation of nitrogen for spirulina hydrothermal carbonization. Bioresour Technol 2019;286:121385. https://doi.org/10.1016/j.biortech.2019.121385.
[26] Liu P, Wang L, Zhou Y, Pan T, Lu X, Zhang D. Effect of hydrothermal treatment on the structure and pyrolysis product distribution of Xiaolongtan lignite. Fuel 2016;164:110–8. https://doi.org/10.1016/j.fuel.2015.09.092.
[27] He C, Wang K, Yang Y, Amaniampong PN, Wang JY. Effective nitrogen removal and recovery from dewatered sewage sludge using a novel integrated system of accelerated hydrothermal deamination and air stripping. Environ Sci Technol 2015;49(11):6872–80. https://doi.org/10.1021/acs.est.5b00652.
[28] He C, Giannis A, Wang J-Y. Conversion of sewage sludge to clean solid fuel using hydrothermal carbonization: hydrochar fuel characteristics and combustion behavior. Appl Energy 2013;111:257–66. https://doi.org/10.1016/j.apenergy.2013.04.084.
[29] Liu X, Zhai Y, Li S, Wang B, Wang T, Liu Y, Qiu Z, Li C. Hydrothermal carbonization of sewage sludge: effect of feed-water pH on hydrochar's physicochemical properties, organic component and thermal behavior. J Hazard Mater 2020. https://doi.org/10.1016/j.jhazmat.2020.122084.
[30] Peng C, Zhai Y, Zhu Y, Wang T, Xu B, Wang T, Li C, Zeng G. Investigation of the structure and reaction pathway of char obtained from sewage sludge with biomass wastes, using hydrothermal treatment. J Clean Prod 2017;166:114–23. https://doi.org/10.1016/j.jclepro.2017.07.108.
[31] Zhang D, Liu P, Lu X, Wang L, Pan T. Upgrading of low rank coal by hydrothermal treatment: coal tar yield during pyrolysis. Fuel Process Technol 2016;141:117–22. https://doi.org/10.1016/j.fuproc.2015.06.037.
[32] Zhou S, Liang H, Han L, Huang G, Yang Z. The influence of manure feedstock, slow pyrolysis, and hydrothermal temperature on manure thermochemical and combustion properties. Waste Manag 2019;88:85–95. https://doi.org/10.1016/j.wasman.2019.03.025.
[33] Wang T, Zhai Y, Zhu Y, Peng C, Xu B, Wang T, Li C, Zeng G. Influence of temperature on nitrogen fate during hydrothermal carbonization of food waste. Bioresour Technol 2018;247:182–9. https://doi.org/10.1016/j.biortech.2017.09.076.
[34] Wang S, Persson H, Yang W, Jönsson PG. Pyrolysis study of hydrothermal carbonization-treated digested sewage sludge using a Py-GC/MS and a bench-scale pyrolyzer. Fuel 2020:262. https://doi.org/10.1016/j.fuel.2019.116335.
[35] Dai L, Wang Y, Liu Y, Ruan R, He C, Duan D, Zhao Y, Yu Z, Jiang L, Wu Q. Bridging the relationship between hydrothermal pretreatment and co-pyrolysis: effect of hydrothermal pretreatment on aromatic production. Energy Convers Manag 2019;180:36–43. https://doi.org/10.1016/j.enconman.2018.10.079.
[36] Cheng Y-T, Huber GW. Production of targeted aromatics by using Diels–Alder classes of reactions with furans and olefins over ZSM-5. Green Chem 2012;14(11). https://doi.org/10.1039/c2gc35767d.
[37] Yang H, Yao J, Chen G, Ma W, Yan B, Qi Y. Overview of upgrading of pyrolysis oil of biomass. Energy Procedia 2014;61:1306–9. https://doi.org/10.1016/j.egypro.2014.11.1087.
[38] Olsbye U, Bjørgen M, Svelle S, Lillerud K-P, Kolboe S. Mechanistic insight into the methanol-to-hydrocarbons reaction. Catal Today 2005;106(1–4):108–11. https://doi.org/10.1016/j.cattod.2005.07.135.
[39] Ma J, Zhang X, Zhao N, Xiao F, Wei W, Sun Y. Mechanism of TBD-catalyzed hydrolysis of acetonitrile. J Mol Struct: THEOCHEM 2009;911(1–3):40–5. https://doi.org/10.1016/j.theochem.2009.06.033.
[40] Watanabe M, Iida T, Inomata H. Decomposition of a long chain saturated fatty acid with some additives in hot compressed water. Energy Convers Manag 2006;47(18–19):3344–50. https://doi.org/10.1016/j.enconman.2006.01.009.
[41] Önal E, Uzun BB, Pütün AE. Bio-oil production via co-pyrolysis of almond shell as biomass and high density polyethylene. Energy Convers Manag 2014;78:704–10. https://doi.org/10.1016/j.enconman.2013.11.022.

[42] Speight G James. Handbook of industrial hydrocarbon processes. 2009. p. 241–79.
[43] Huang H-j, Chang Y-c, Lai F-y, Zhou C-f, Pan Z-q, Xiao X-f, Wang J-x, Zhou C-h. Co-liquefaction of sewage sludge and rice straw/wood sawdust: the effect of process parameters on the yields/properties of bio-oil and biochar products. Energy 2019;173:140–50. https://doi.org/10.1016/j.energy.2019.02.071.
[44] Zhou J, Liu S, Zhou N, Fan L, Zhang Y, Peng P, Anderson E, Ding K, Wang Y, Liu Y, Chen P, Ruan R. Development and application of a continuous fast microwave pyrolysis system for sewage sludge utilization. Bioresour Technol 2018;256:295–301. https://doi.org/10.1016/j.biortech.2018.02.034.
[45] Zhai Y, Peng C, Xu B, Wang T, Li C, Zeng G, Zhu Y. Hydrothermal carbonisation of sewage sludge for char production with different waste biomass: effects of reaction temperature and energy recycling. Energy 2017;127:167–74. https://doi.org/10.1016/j.energy.2017.03.116.